Part 1 – Reverse-Engineer a Published TFLN Modulator

For this part of the challenge, we chose to analyse the electro-optic (EO) modulator reported in the paper "*1.1-cm-long thin-film lithium niobate Mach-Zehnder modulator with low driving voltage integrated by micro-transfer printing*".

Summary

In this work, the authors report on the integration of a thin-film lithium niobate (TFLN) Mach-Zehnder Inteferometer (MZI) on a silica-on-silicon substrate via micro-transfer printing. The MZI is first etched on a 600 nm-thick-X-cut TFLN layer prepared on top of a SiO_2 layer on a silicon wafer. Owing to tether structures, the silica can be etched with hydruofluoric acis (HF), resulting in free standing TFLN coupons. The coupons are then pick-up using PDMS and printed/bonded to the final wafer. The main novelty is the length of 11 mm achieved with the micro-transfer printing method.

Device configuration

Figure 1 shows a Mach–Zehnder interferometer (MZI) modulator. Continuous-wave light at 1550 nm is edge-coupled into the chip and split into two waveguide arms by a multimode interferometer (MMI). After propagating through the two arms, the fields are recombined by a second MMI. The output power is set by the differential optical phase between the arms, yielding constructive or destructive interference.

The cross section of the MZI arms is shown in Figure 2, with the relevant dimensions summarized in Table 1.

Working principle

Phase control in the MZI arms is achieved electro-optically. The electrodes implement a ground–signal–ground (GSG) layout with the signal electrode between the two arms and ground electrodes on the outer sides. A voltage on the signal electrode produces electric fields of opposite direction in the two arms, enabling push–pull drive. Through the Pockels effect in thin-film lithium niobate (TFLN), these opposite fields induce refractive-index changes of opposite sign, generating a differential phase shift and thereby modulating the output intensity from a minimum (ideally zero at destructive interference) to a maximum (constructive interference).

For high-speed operation at radio frequencies (RF), the electrodes are designed as a travelling wave transmission line. The microwave propagates along the electrodes, while the optical waves co-propagate in the waveguides. This ensures that the modulation interaction is distributed continuously along the device length.

EO efficiency is mainly characterized by the product $V_\pi \cdot L$, where V_π is the voltage needed to generate a phase difference of π between the arms and L is the device length. It depends mainly on three factors:

(i) EO coefficient: quantifies how much the refractive index changes for a given applied electric field. Lithium-niobate has a large r , especially along its Z axis (extraordinary index direction).
(ii) RF-optical overlap factor: the refractive index change is proportional to the overlap between the RF mode and the optical mode.
(iii) Electrode gap: smaller gaps lead to higher electric fields, increasing the refractive index change. As a trade off, the optical losses can increase if the electrodes are too close to the waveguide.

Important factors that limit the bandwidth of MZIs:

(i) Velocity mismatch between RF and optical waves: for RF modulation, it is crucial that the microwave and the optical wave co propagate with the same speed. If there is a velocity mismatch, the phase modulation is not correctly distributed throughout the device length, leading to improper modulation at high frequencies. Longer devices enhance the effect of velocity mismatch.
(ii) RF losses in the electrodes: due to conductor loss and dielectric loss in the surrounding materials. These losses also scale with the device length and with the RF frequency.

The most critical fabrication tolerances for the EO efficiency and the bandwidth are:

(i) Waveguide width and etch depth: define the mode distribution and the group index, which in turn affect the optical-RF overlap (EO efficiency) and the velocity matching (bandwidth), respectively.

(ii) Electrode gap: changes EO efficiency by changing the electric field and can increase losses if fabrication imperfections result in an electrode being too close to a waveguide.

(iii) Electrode dimensions: changes the impedance of the RF line and the effective index of the propagating microwave, leading to velocity mismatching.

(iv) Side wall roughness: large impact on optical loss.

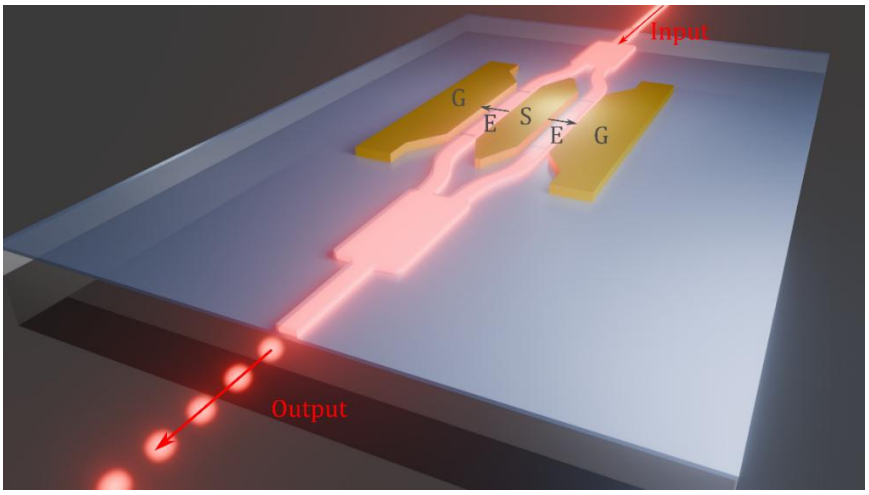

Figure 1 - Illustration of a TFLN MZI with electrodes in a GSG configuration. The light is coupled into the chip via edge coupling. The output is modulated by the voltage applied to the signal electrode in between the waveguides.

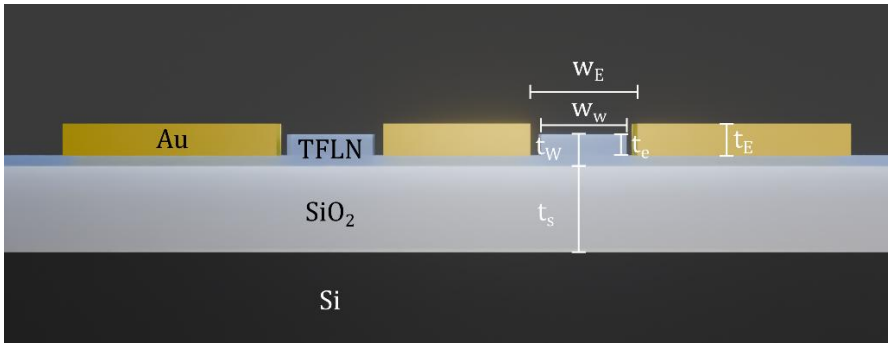

Figure 2 - Waveguide and electrode cross sections of the MZI arms.

w_w, waveguide width	2.3 µm	t_w, waveguide tchinkess	600 nm
t_e, etch depth	400 nm	t_E, electrode thickness	1.2 µm
w_g electrode gap width	5 µm	t_s, bottom oxide thickness	3 µm

Table 1 - Relevant dimensions of the MZI cross section shown in Figure 2.

Device performance

The optical loss in the waveguides is characterized by the cutback method, resulting in a measured loss of 0.7 dB/cm attributed to sidewall roughness. The loss in each MMI is simulated to be 0.1 dB. For the longest device characterized in the paper, both loss contributions result in a total insertion loss of 0.97 dB.

The product $V_\pi \cdot L$ = 2.7 V-cm is reported for the device with length L = 9.9 mm. This value is larger than the simulated 2.5 V-cm, which the authors attribute to fabrication errors.

The bandwidth is measured for two different devices. The 3-dB bandwidth of a device with L = 3 mm exceeds 50 GHz. The measurement is limited by the Vector Network Analyzer (VNA) used by the authors. The 3-dB bandwidth of a device with L = 9.9 mm was approximately 28 GHz. The bandwidth was limited by (i) the mismatch of group indices for optical and microwave (2.2 and 2.1, respectively), (ii) low impedance of 40 Ω of the GSG electrodes, (iii) large microwave absorption of the non-doped silicon substrate.

Part 2 – Simulation

Simulation flow diagram

In this part of the challenge, we simulate the device analyzed in Part 1. The simulation flow is shown in Figure 3.

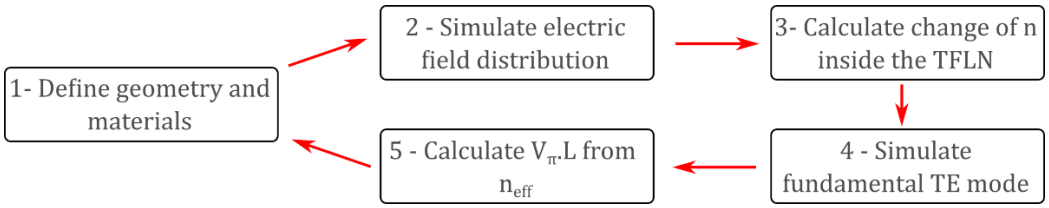

Figure 3 - Simulation diagram.

1) The first step is to define the geometry of the cross section to be simulated and the material of each component. The simulated cross section can be found in Figure 2.
2) The second step is to simulate the electric field E(x,z) in the xz plane for a given applied voltage V_x. Here, we use an x cut TFLN, meaning the X-direction of the crystal is perpendicular to the plane. Furthermore, we consider that the Z-direction of the crystal is aligned with the x axis of the simulation, such that (i) the TE mode of the waveguide experiences the extraordinary refractive index of lithium niobate and (ii) the EO coefficient is maximal along the x axis. For the simulation of E(x,z) the DC relative permittivities are 27.9, 44.3 and 44.3, respectively along x, y and z, respectively.
3) In the third step, we use E(x,z) to calculate the change in refractive index Δn(x,z). In general, the change in the refractive index tensor is described by

$$\Delta\left(\frac{1}{n^2}\right)_{ij} = \sum_k r_{ijk} E_k$$

Where r_{ijk} is the Pockels tensor with 27 components and E_k is the electric field along the axis k. We can simplify this expression by considering:

(i) The field propagates along one of the ordinary axes of the uniaxial birefringent material, with polarization along the extraordinary axis → we only have to consider diagonal perturbations.
(ii) The symmetry of the lithium niobate crystal forces many of the tensor elements to be zero.
(iii) We consider that the electrodes an electric field mainly along the x axis, such that $E_x \gg E_y, E_z$.
(iv) The perturbation is small, such that $\Delta\left(\frac{1}{n^2}\right) \approx n - \frac{n^3}{2} rE$

Applying these assumptions, we can write:

$$\begin{cases} n_x = n_e - \dfrac{n_e^3}{2} r_{33} E_x \\ n_y = n_o - \dfrac{n_o^3}{2} r_{13} E_x \\ n_z = n_o - \dfrac{n_o^3}{2} r_{13} E_x \end{cases}$$

With $n_e = 2.14$, $n_o = 2.21$, $r_{13} = 9.6 \times 10^{-12}\ V^{-1}$ and $r_{33} = 30.9 \times 10^{-12}\ V^{-1}$.

With these equations we calculate $n_x(x,z), n_y(x,z), n_z(x,z)$, which we use in the next step. We note that the assumptions we made limit the accuracy of the simulation in the case in which the X crystal direction is not perfectly perpendicular to the substrate, or the waveguides are fabricated such that the TE mode is not exactly polarized along the Z crystal direction. They are also not accurate for TM waves, for which the electric field has components along two different axes (y and z). Finally, the approximations are also limited by the fact that the electrodes also create an electric field component along z.

4) In the fourth step we simulate the fundamental mode of the waveguide considering the pointwise change in refractive index. From this simulation we extract the effective index n_{eff} of the TE mode.

5) In the fifth and final step, we use the effective index to calculate the calculate the length L_π needed to get a phase difference of π between the arms in the push and pull configuration (GSG electrodes):

$$\frac{2\pi}{\lambda} n_{eff}(V) L_\pi - \frac{2\pi}{\lambda} n_{eff}(0) L_\pi = \frac{\pi}{2}$$

$$L_\pi = \frac{1}{2} \frac{\lambda}{2|n_{eff}(V) - n_{eff}(0)|}$$

Finally, we calculate $V_\pi \cdot L = V_x \times L_\pi$.

The geometry is then updated, and the simulation starts back from step 1.

Simulation results

We use Lumerical CAHRGE and FEEM to perform the simulations. We assume a sidewall angle of 90 degrees, as it is assumed in the reference paper. A sidewall angle of 60 degrees would be typical in real devices.

The electric field components generated by $V_x = 1\ V$ are shown in Figure 4. At the center region of the waveguide we have $E_x \approx 10^5 \gg E_y, E_z$, validating the approximations described in the previous sections. Note that the value of E_x is on the same order of magnitude as the expected field $1\ V/5\ \mu m \approx 2 \times 10^5\ V/m$.

The three components of the fundamental TE mode simulated for $V_x = 0\ V$ are shown in Figure 5. Once again, the x component dominates over the other two components (notice the difference in scale bar). The effective refractive index change with respect to $V_x = 0\ V$ is $\Delta n_{eff} = 1.59 \times 10^{-5}$.

From the values of Δn_{eff} we calculate $V_\pi \cdot L = 2.43\ V \cdot cm$, in good agreement with the simulated value reported on the paper.

Next, we consider that the electrode gap is used to tune $V_\pi \cdot L$. Figure 6a shows $V_\pi \cdot L$ as a function of w_E, showing a decrease in this particular metric with increasing w_E. This is consistent with the fact that $E_x \sim w_E^{-1}$ for a given V_x, resulting in $V_\pi \cdot L \sim w_E$. This dependence is particular important if the electrodes are fabricated by standard lithography. In such a case, a precision of $\sim 1\ \mu m$ can be expected, which, for a nominal $w_E = 5\ \mu m$ can generate variations of ± 20 % in the value of $V_\pi \cdot L$.

Then, we consider the effect of dimension variations from fabrication imperfections. Figure 6b shows $V_\pi \cdot L$ as a function of the waveguide thickness t_w, with variations of $\pm 20\ nm$ relative to the nominal $t_w = 600\ nm$. This results in variations of ± 2 % in $V_\pi \cdot L$.

Figure 6c shows $V_\pi \cdot L$ as a function of the waveguide width w_w, with variations of $\pm 150\ nm$ relative to the nominal $w_w = 2.3\ \mu m$. This results in variations of ± 2.5 % in $V_\pi \cdot L$.

Finally, we perform 450 simulations where (w_E, w_W, t_W) are sampled from independent normal distributions with mean $(5, 2.3, 0.6)\ \mu m$ and standard deviation $(1, 0.15, 0.02)\ \mu m$. The resulting histogram of $V_\pi \cdot L$ is shown in Figure 7. A fit to a normal distribution shows an average value of $2.43\ V.cm$ and a standard deviation of $0.58\ V.cm$.

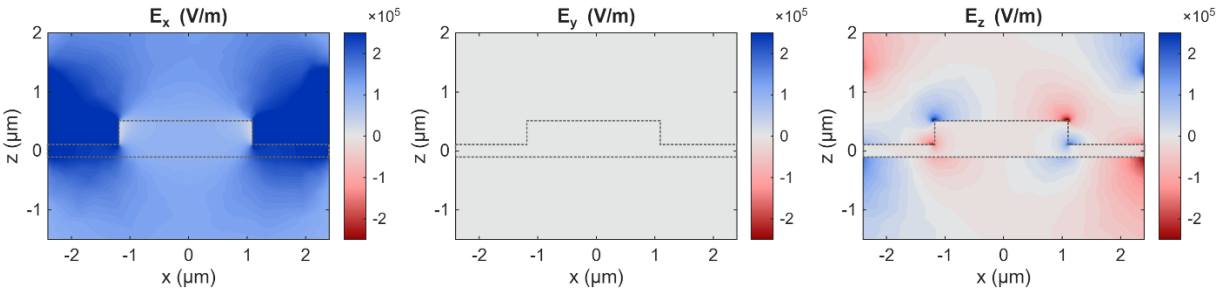

Figure 4 - Electric field components for $V_x = 1V$.

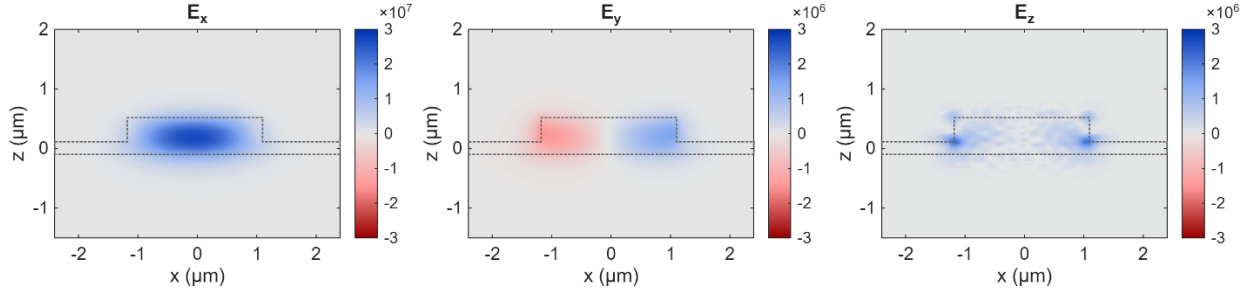

Figure 5 - Electric field components of the fundamental TE mode.

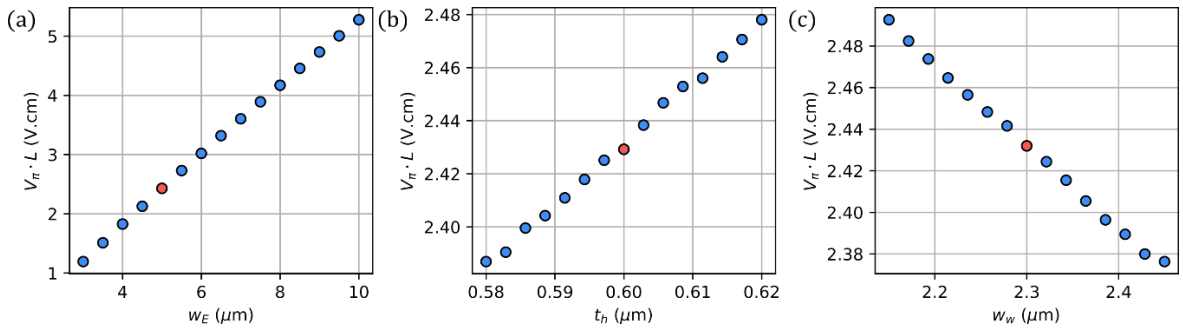

Figure 6 - $V_\pi \cdot L$ as a function of (a) Electrode gap, (b) waveguide thickness and (c) waveguide width. The red points are the nominal values.

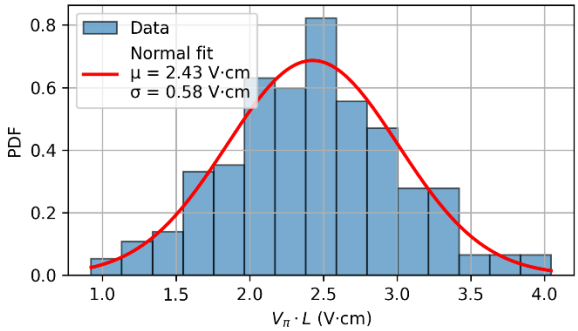

Figure 7 - Histogram of $V_\pi \cdot L$ over 450 simulated devices. The values of (w_E, w_W, t_W) are sampled from independent normal distributions with mean $(5, 2.3, 0.6)$ μm and standard deviation $(1, 0.15, 0.02)$ μm. The sampled points with $w_E < w_w + 200$ nm are excluded.

Part 3 – PDK Building Block Definition

Component: TFLN_MZM_STD_50G					
Summary: Thin film lithium niobate travelling wave Mach Zehnder modulator. Bandwidth: 50 GHz. Wavelength: C-band (nominal 1550 nm), TE polarization. Electrode configuration GSG, 50 Ω terminated.					
Material stack					
100Layer		Material	Thickness	Tolerance	
Substrate		Si	530	±25	µm
Bottom oxide		Thermal SiO_2	3	±0.1	µm
Device layer		TFLN, x-cut	600	±20	nm
Electrode		Au	0.5 – 1.5	±0.05	µm
Physical parameters					
Parameter	Symbol	Nominal	Valid range	Tolerance	Unit
Waveguide width	w_w	2.3	1.8 – 2.5	±0.05	µm
Waveguide thickness	t_w	600	Fixed	±20	nm
Etch depth	t_e	400	200-500	±20	nm
Electrode gap	w_E	5	3 – 10	±0.5	µm
Electrode thickness	t_E	1.2	0.5 – 1.5	±0.05	µm
Arm length	L	10	1-10	±0.001	mm
Optical characteristics					
Quantity	Range				Unit
Waveguide loss	< 0.5				dB/cm
MMI loss	< 0.1				dB
Return loss	> 40				dB
Extinction ratio	> 20				dB
Electrical characteristics					
Quantity	Range				Unit
Impedance	50±5				Ω
RF propagation loss	<1.8 @50 GHz				dB/cm
RF bandwidth (3 dB)	> 70				GHz
Nominal performance *					
Performance indicator	Nominal value		Tolerance		Unit
V_π	3.0		±0.5		V
$V_\pi \cdot L$	3.0		±0.5		V.cm
EO bandwidth (3 dB)	50		±5		GHz
Max. NRZ data rate	≥ 45		-		Gb/s
Max. PAM4 data rate	≥ 90		-		Gb/s

** The nominal performance is specified at the nominal physical parameters, wavelength of 1550 nm, TE polarization and operating temperature T = 30 °C.*

Cross section and footprint: